Industrial Turbo-Assisted Direct Solar Air Heater Using Linear Fresnel Concentrating Collectors

Antonio Famiglietti[1], Antonio Lecuona-Neumann[1], Mohammad Rahjoo[1] and José Nogueira-Goriba[2]

1 Universidad Carlos III de Madrid, Departamento de Ingenieria Termica y de Fluidos, Grupo ITEA, Leganés (Spain),
2 Universidad de Castilla La Mancha, Campus de Excelencia Internacional en Energia y Medioambiente, Escuela de Ingenieria Industrial y Aeroespacial, Toledo (Spain)

Abstract

Among the solar technologies nowadays considered as renewable energy sources for industrial processes, concentrating solar collectors are receiving growing attention due to their capability of providing heat at higher temperatures than other solar collectors. This study focuses on the application of linear Fresnel collectors to directly produce hot air in the medium temperature range 150 °C - 400 °C for industrial processes, aiming at low cost. An innovative layout is proposed. Air is used as heat transfer fluid inside the solar receiver, a low-cost commercial turbocharger is used to compress ambient air through the plant, extracting from the solar source the required pumping power with the attached turbine, minimizing auxiliary energy consumption. A *turbo-assisted direct solar air heater* of medium-scale size is designed and simulated along representative days of a typical meteorological year, in order to assess the concept, its performances and relevant technical aspects. The study confirms its technical feasibility either in summer and winter season for the selected location (Madrid, Spain). The system provides an hot air stream between 300°C and 400°C without external energy consumption for pumping, avoiding the receiver tube overheating.

Solar Air Heater, Solar Heat for Industrial Processes, SHIP, Concentrating Solar Heat, Linear Fresnel collector

1. Introduction

Industry accounts for 38% of the final energy consumption worldwide (International Energy Agency 2018). The large thermal energy demand for industrial processes covers a broad range of temperatures, customarily: the low-temperature range T < 150 °C, the medium temperature range 150 °C < T < 400 °C, and the high-temperature range T > 400 °C. (Sharma et al. 2017) states that 60% of industrial energy heat demand is between 30 and 250 °C. Most of exiting Solar Heat for Industrial Processes, SHIP, installation are in the low-temperature range where flat plate collectors FPCs or evacuated tubes collectors ETCs can be used (Mekhilef, Saidur, and Safari 2011). Concentrating solar heat CSH can be provided at higher temperatures using parabolic trough collectors PTCs or linear Fresnel collectors LFCs. Industrial CSH existing plants are reported in (Sharma et al. 2017) as well as in (SHIP Database). PTC, and with a lesser extend LFC, are used for steam production, industrial refrigeration coupled with absorption chillers, water heating and process heating. Almost all of them use liquid heat carrying fluids.

Industrial processes using air as a heat-supplying fluid are widespread. Among them, drying and air preheating are high energy-demanding processes, common to several industrial sectors, as food and beverage, chemical, pulp and paper, residues and wastewater treatments, among others. Temperature requirements vary with the specific application, from low to medium temperature ranges. For such applications, this study evaluates a novel open circuit to atmosphere OCA direct solar air heater. It provides hot air up to 350 °C using off-the-shelf concentrating collectors. The herewith studied technology avoids the cost, weight, hurdle, environmental impact, and risks of liquid heat-carrying liquids. Moreover, it avoids the use of heat exchangers.

2. Turbo-assisted direct solar air heater

The *Turbo-assisted direct air heater*, T-SAH, is a unique technology (Lecuona-Neumann 2016) able to heat ambient air up to the medium temperature range using concentrating solar collectors, as linear Fresnel collector

Selection and/or peer review under responsibility of Scientific Committee
doi:10.18086/eurosun.2020.03.06 Available at http://proceedings.ises.org

LFC, or Parabolic Trough collector PTC, not requiring the use of conventional heat transfer fluid HTF (e.g., thermal oil, water, …) and an heat exchanger HX for heat delivery, improving the flexibility and safety, besides to reduce cost.

Due to its physical properties, air at ambient conditions is not appropriate as a heat carrier. Internal heat transfer rate occurring between the solar receiver wall and the internal airflow is modest compared to other HTFs, and as a result, the wall over-temperature is high. The relatively low air density and specific heat capacity turn into high mean flow velocities required to limit the outlet temperature. This is necessary to avoid receiver wall overheating, especially under high solar heat flux conditions, (i.e., large collector aperture and length, and/or high solar irradiance). The pumping power required to overcome the total pressure drops across the receiver and piping can be in the same order of magnitude of the captured solar power, which comes from high auxiliary energy consumption.

In the proposed layout, Fig.1, an automotive turbocharger is used to alleviate or eliminate these drawbacks and even convert them into an advantage. Ambient air is pressurized before entering the collector using a compressor *c*. Compressing power is recovered by the attached expander *e* after heating. For a given mass flow rate required to remove heat from the receiver, the increase in density obtained thanks to compression translates into lower the mean velocities, minimizing the pressure drop across the receiver and the pumping power required, in spite of the increase of temperature through the compressor. The compressor and the turbine expander are mechanically coupled as in a Brayton cycle configuration. Since no net mechanical work is expected to be extracted at the shaft, an automotive turbocharger is used. If there is mechanical power left, it will be in the outlet flow.

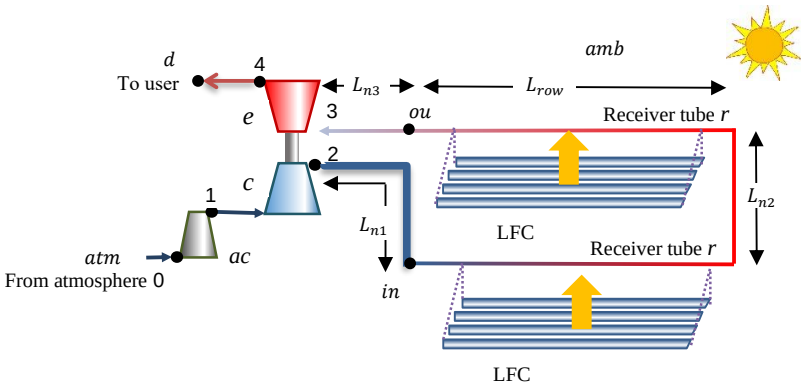

Fig. 1: Turbo-assisted direct solar air heater concept using LFCs, $n_s = 2$ and $n_p = 1$.

As long as turbocharger freewheeling is achieved, no external power is needed to pump air throughout the collector, since the turbine can drive the compressor, providing the compressing and the pumping power required. An auxiliary compressor can supply the pumping power during starting transient, cloudy transients, as well as for control purposes, avoiding overheating. Air exits the turbine at 300 - 400 °C. (Famiglietti et al. 2020) presents a generic theoretical investigation on the proposed layout, including numerical modeling, critical parameters and performance assessment.

According to the mentioned layout, a small to the medium-scale facility has been modeled and simulated in the present work. A solar field has been configured combining commercial LFCs in parallel and series layout in order to suitably match with a specific turbocharger. The single LFC module is $L_m = 5.28$ long, having an aperture of $W_a = 5$ m and a reflective surface of $A_m = 26.40$ m^2. A series of $n_s = 6$ modules are aligned to obtain a U-loop, while $n_p = 4$ U-loops are connected in parallel to the single turbocharger. The U-loop length is a good compromise between the need to capture enough solar power to produce useful outlet temperatures and the need to keep small pressure drops across the loop. Additionally, too short series would result in relatively high optical end losses at the collector rows extremities. 4 U-loops in parallel guarantee enough mass flow rate, matching the operative range of increased size turbochargers, which results in high-performance. The solar field axis N-S oriented, results in an overall capturing surface of 633.6 m^2, which is a small/medium scale plant suitable for industrial applications.

3. Numerical model

The LFCs field has been modeled using the peak optical efficiency $\eta_{op0} = 0.63$ given by the manufacturer (Solatom, n.d.), applying the incident angle modifiers $IAM_T\langle\theta_T\rangle$ and $IAM_L\langle\theta_L\rangle$ for taking into account the optical losses related to transversal and longitudinal components of sun rays incidence angle (Karathanasis 2019). The solar power incident at the collector tube axis $\dot{Q}_s$ results as in eq. (1).

$$\dot{Q}_s = G_{bn} IAM_T\langle\theta_T\rangle IAM_L\langle\theta_L\rangle \eta_{op0} W_a L_m n_s n_p \quad \text{(eq.1)}$$

Optical end losses, due to the concentrated radiation impacting out of the tube length are taken into account through the end losses factor $f_{end}\langle\theta_L\rangle = \dot{Q}_r/\dot{Q}_s$, (Heimsath et al. 2014) being $\dot{Q}_r$ the net solar power impacting on the solar receiver tube.

A steady-state model of receiver tube is obtained using the heat removal factor F_R and efficiency factor F' as proposed by (Duffie, Beckman, and McGowan 1985), for what the useful power transferred to air across the tube length L becomes $\dot{Q}_u$, which is used to heat the air flow rate $\dot{m}$:

$$\dot{Q}_u = F_R L P_{ex}[\dot{q}_s - U_L(T_{in} - T_{amb})] = \dot{m}(c_{p,ou} T_{ou,t} - c_{p,in} T_{in,t}) \quad \text{(eq.2)}$$

$$F_R\langle\dot{m}\rangle = \frac{\dot{m}c_p}{LP_{ex}U_L}\left[1 - \exp\left(-\frac{LF'P_{ex}U_L}{\dot{m}c_p}\right)\right]; \qquad F' = \frac{1}{1 + \frac{U_L P_{ex}}{h_a P}} \quad \text{(eq.3)}$$

The solar heat flux is obtained from eq.(1) as $\dot{q}_s = G_{bn} IAM_T\langle\theta_T\rangle IAM_L\langle\theta_L\rangle \eta_{op0} W_a P_{ex}^{-1}$, being P_{ex} and P the external and internal tube perimeters, U_L the heat transfer coefficient from the tube wall to ambient, $T_{in,t}$ and $T_{ou,t}$ are the stagnation temperatures at the tube inlet and outlet respectively, h_a is the internal wall to air heat transfer coefficient. The value of U_L for any tube wall temperature is obtained from the thermal losses test performed by (Burkholder and Kutscher 2008) on a usual evacuated tube with an external diameter $D_{ex} = 0.07$ m, equipped with selective coating. Discretization is applied to the overall receiver length to increase accuracy.

A turbocharger model is due to computing the system. Under steady-state conditions, the turbine and the compressor, which are connected by the shared shaft, hold the mechanical balance when eq. (4) is verified. This means that the power generated by air expansion through the turbine $\dot{W}_e$ is able to drive the compressor that consumes the power $\dot{W}_c$, considering a mechanical efficiency at the shaft η_m. Under this condition, the turbocharger run at the constant rotational speed n_T without external auxiliary energy consumption. For the proposed layout, it means that the compressor is able to pump air through the solar field without consuming external energy, thus in autonomous mode, while at the turbine outlet airflow holds the medium temperature range, useful for industrial usage in thermal processes.

$$\dot{W}_e \eta_m - \dot{W}_c = \dot{W}_{net} = 0 \quad \text{(eq. 4)}$$

According to the cycle points reported in Fig. 1, the compressor and turbine powers can be obtained from isoentropic total to total efficiencies η_e and η_c, pressure ratios $\pi_c = \frac{p_{2t}}{p_{1t}}$ and $\pi_e = \frac{p_{3t}}{p_{4t}}$, and inlet stagnation temperatures T_{1t} and T_{3t} , respectively for the compressor eq. (5) and the turbine eq. (6), where $\gamma = c_p/c_v$.

$$\dot{W}_c = \dot{m}c_{p,c} T_{1t}\left(\pi_c^{\frac{\gamma_c - 1}{\gamma_c}} - 1\right)\eta_c^{-1} \quad \text{(eq. 5)}$$

$$\dot{W}_e = \dot{m}c_{p,e} T_{3t}\left[1 - \pi_e^{-\frac{\gamma_e - 1}{\gamma_e}}\right]\eta_e \quad \text{(eq. 6)}$$

The total temperature at the receiver tube inlet results from eq. (7). Air is available for usage at turbine exit temperature T_{4t}, as in eq. (8).

$$T_{2t} = T_{1t}\left[1 + \left(\pi_c^{\frac{\gamma_c - 1}{\gamma_c}} - 1\right)\eta_c^{-1}\right] \quad \text{(eq. 7)}$$

$$T_{4t} = T_{3t}\left[1 - \eta_e\left(1 - \pi_e^{-\frac{\gamma_e - 1}{\gamma_e}}\right)\right] \qquad \text{(eq. 8)}$$

Compressor performance can be described using two relations $\pi_c = \pi_c\langle \dot{m}, T_{in}, n_T \rangle$ and $\eta_c = \eta_c\langle \dot{m}, T_{in}, n_T \rangle$, which can be extrapolated from compressor performance maps provided by the manufacturers, (Guzzella and Onder 2010). Following the same approach, the relation $\dot{m}\langle \pi_e \rangle$ for the turbine is extrapolated from the map given by the manufacturer. A turbine efficiency model $\eta_e\langle n_T, \pi_e \rangle$ is implemented following (Guzzella and Onder 2010). The turbomachines performance model, together with the collector and receiver model above described, enables to determine the operative point for the system under steady-state conditions, according to solar position and irradiance at given ambient conditions. Autonomous operations, or freewheeling, is achieved when eq. (4) is verified. On the other hand, the receiver tube thermal limit indicated at 600 °C by most manufacturers should not be overcome. A good matching between the solar field and the turbocharger can be obtained by selecting the suitable turbocharger size among the available models on the market, so that the limited operating range of compressor and turbine, indicated by their performance maps, fits the solar power variation along the day and the year.

4. Results

The *turbo-assisted solar air heater* herewith proposed has been simulated on typical representative days of the year, extracted from the Typical Meteorological Year TMY (Habte et al. 2017) for the location of Madrid (Spain).

Fig.2 reports performances during a typical summer day with a clear sky in July. In Fig 2(a) direct solar normal irradiance G_{bn} is shown across true solar time TST, together with incident angle modifiers and the optical end losses factor f_{end}, as they determine the solar power at the receiver tube $\dot{Q}_r$. It can be noted that either f_{end} and IAM_L reaches values close to unity due to the high sun elevation at midday in summer. It follows that the end losses $\dot{Q}_{fend} = \dot{Q}_s - \dot{Q}_r = \dot{Q}_s(1 - f_{end})$ are moderate, in spite of the relatively short collector rows, as reported in Fig. 2(b). $\dot{Q}_s$ and $\dot{Q}_r$ are also reported, as well as the power delivered to the user $\dot{Q}_a = (T_4 c_{p,a} - T_{amb} c_{p,amb})\dot{m}$. Thermal losses from the receiver tubes as well as connection pipes L_{n1}, L_{n2}, L_{n3} are estimated as $\dot{Q}_L = \dot{Q}_r - \dot{Q}_a$. The solar power available during the day on an equivalent solar field surface normal to sunrays $\dot{Q}_{bn} = G_{bn} L_m W_a n_s n_p$ is reported. It can be noted that the system is not operating during the overall daylight time interval, since it is shut off during the first and the last hours of the day when the solar power is low. In fact, under low irradiance conditions is not possible to find freewheeling. This is mainly due to the compressor operating range not yielding enough efficiency at very low mass flow rates, as it is required at low irradiance conditions. A load factor $LF = \dot{q}_s / \dot{q}_{s,max}$ can be defined as the ratio between the solar heat flux at the receiver and its maximum value expected across the year, with $\dot{q}_{s,max} = 13{,}500\ \mathrm{Wm^{-2}}$. Below a certain load factor, the system does not operate in autonomous mode and is considered as shut off in the present simulation. The threshold load factor LF_{th} resulted in being around 0.3 for the turbocharger and solar field layout considered. The load factor is reported in Fig 2(b).

Fig.2 (c) shows the temperature of the main points of the circuit, as indicated in Fig.1. Outlet compressor temperature is affected by the compression ratio, eq. (7), and varies across the day, reaching 150 °C as maximum. T_3 results from the power gained $\dot{Q}_u$, eq. (2), across the receiver tube by the airflow. It must be high enough to provide the required power at the turbine but ensuring that the maximum wall temperature allowed $T_{w,max}$ is not overcome. Wall temperature corresponding to the tube end T_{w3} is reported, confirming that $T_{w3} < T_{w,max} = 600$ °C. Surprisingly, the air temperature at the turbine outlet delivered to the user T_4 shows a relatively flat profile along the operating hours, between 350 °C and 380 °C. This can be considered very favourable. The mass flow rate varies across the day between $0.3\ \mathrm{kg/s}$ and $0.65\ \mathrm{kg/s}$, according to the turbocharger maps. In fact, the variation of solar power affects the inlet turbine temperature, hence the provided $\dot{W}_e$, bringing the turbocharger to modify its operating point. Higher solar power leads the turbocharger to operate at higher speeds, hence with higher mass flow rates and pressure ratios, Fig.2 (c)-(d). Isoentropic efficiencies, also reported, keep close to the maximum values across the operating hours. Turbocharger speed is reported in terms of corrected speed $n_{c,cor} = n_T \sqrt{T_{c,ref} T_1^{-1}}$, with $T_{c,ref} = 302.6\ \mathrm{K}$ over the maximum $n_{c,cor}^{max} = 87{,}986$ rpm for the selected turbocharger, being $n_{c,cor}^{min} = 27{,}960$ rpm.

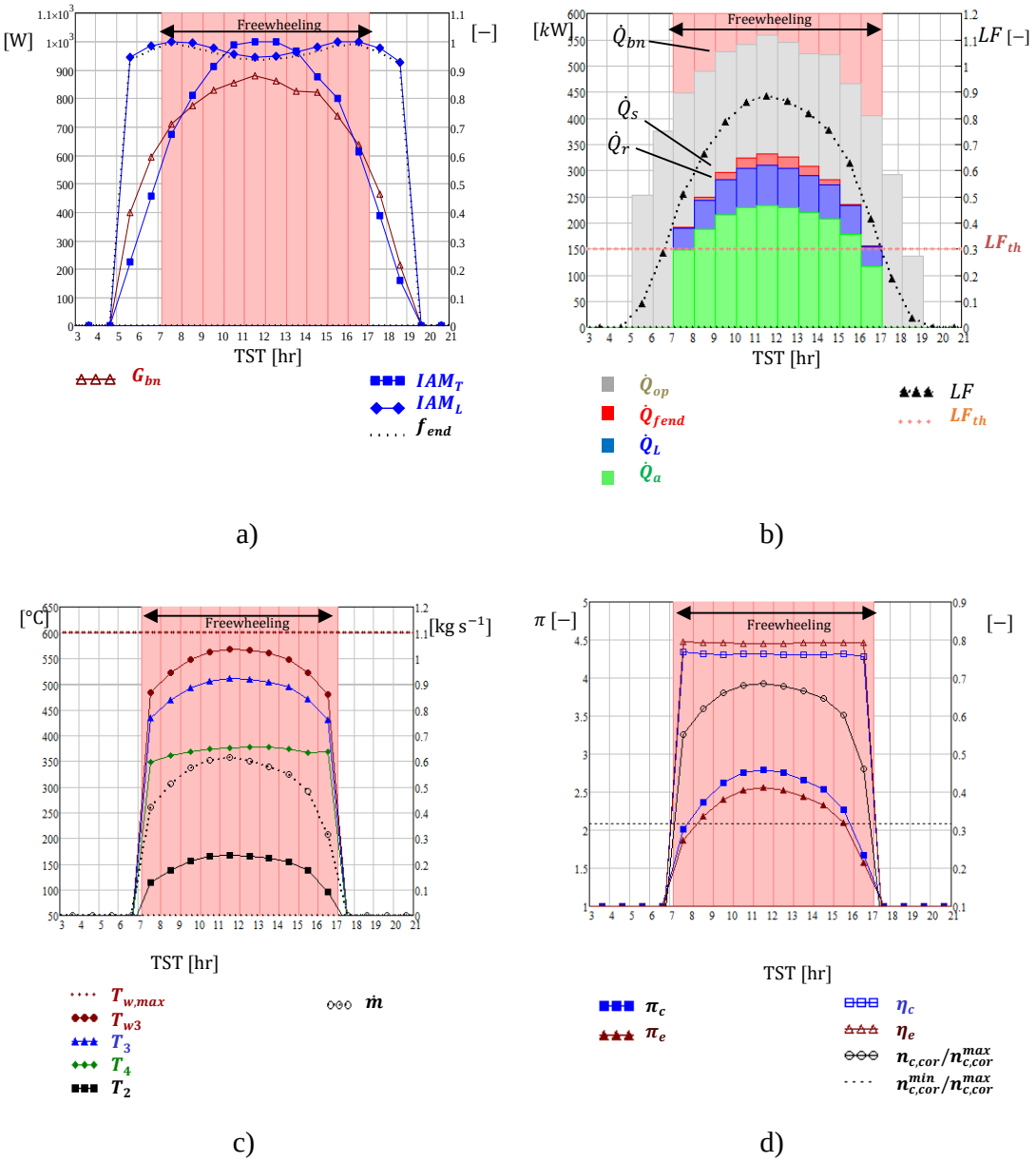

Fig.2 Performance in a clear summer day, Madrid (Spain).

Performances during a typical day with clear sky in March are representative of the intermediate seasons, Fig.3. The lower sun elevation results in lower optical efficiency, being the incident angle modifier lower than in the summer case. End losses are also more significant. The load factor, Fig.3(b) is lower than LF_{th} either in the morning and afternoon. Operative hours are reduced with respect to the summer case, but the system can produce hot air in the central hours of the day. On the other hand, the output air temperature remains higher than 300 °C, fulfilling the scope of medium temperature heat production, Fig.3(c).

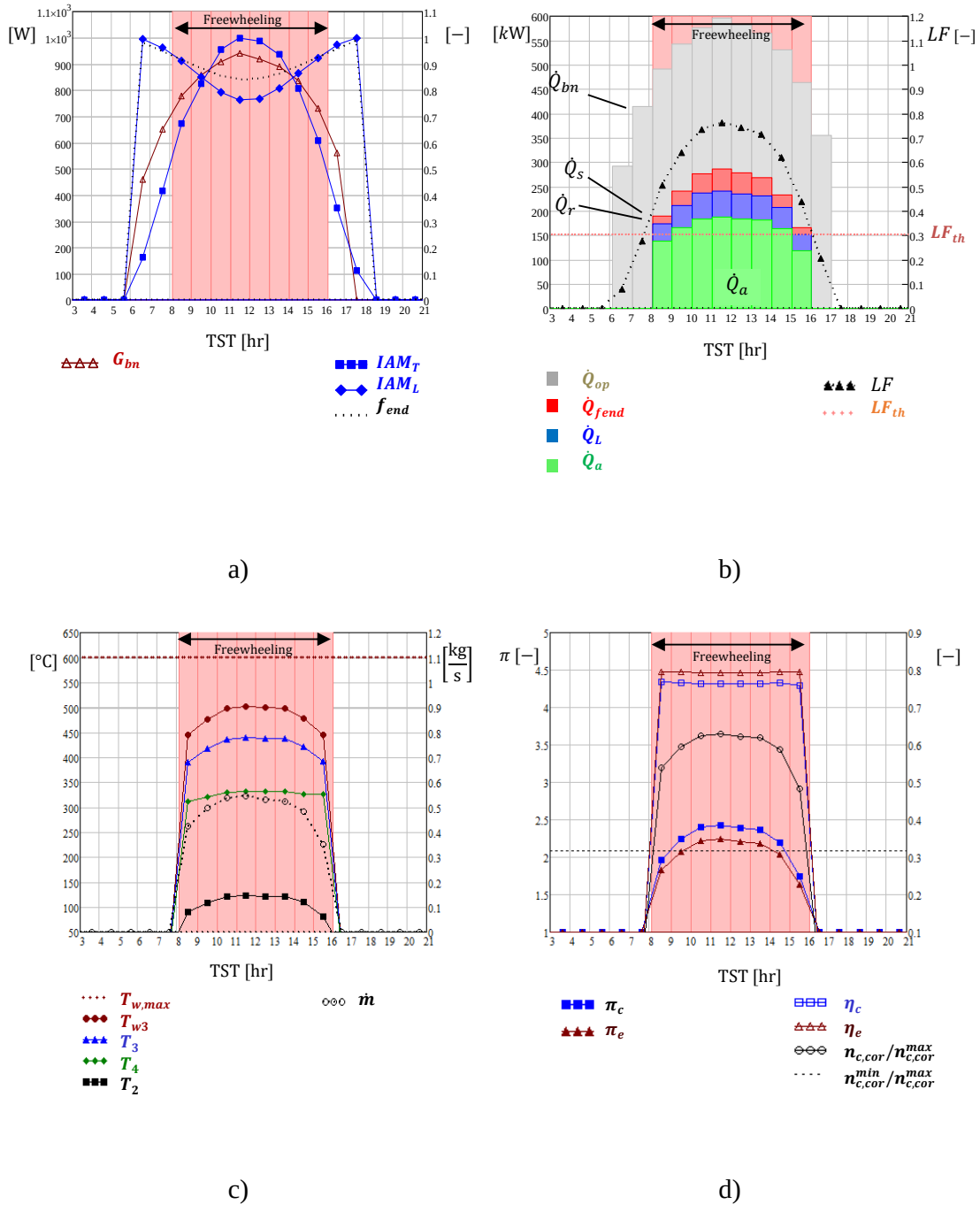

Fig.3 Performance in a clear spring day, Madrid (Spain).

In addition to the above numerical experiments, the behavior of the T-SAH is investigated for a typical winter day of December, with a clear sky. Fig. 4 depicts the performances. It can be noted as the optical efficiency is reduced due to lower IAM_L and f_{end}, with respect to the previous cases. As indicated in Fig.4(b), only for a few hours of the day, the load factor overcomes the threshold value, and the system operates in freewheeling. The power delivered is modest while the optical end losses increase in relative terms. The delivered airflow holds a temperature above 300 °C, although the mass flow rate is modest, as well as the pressure ratios, Fig. 4(c).

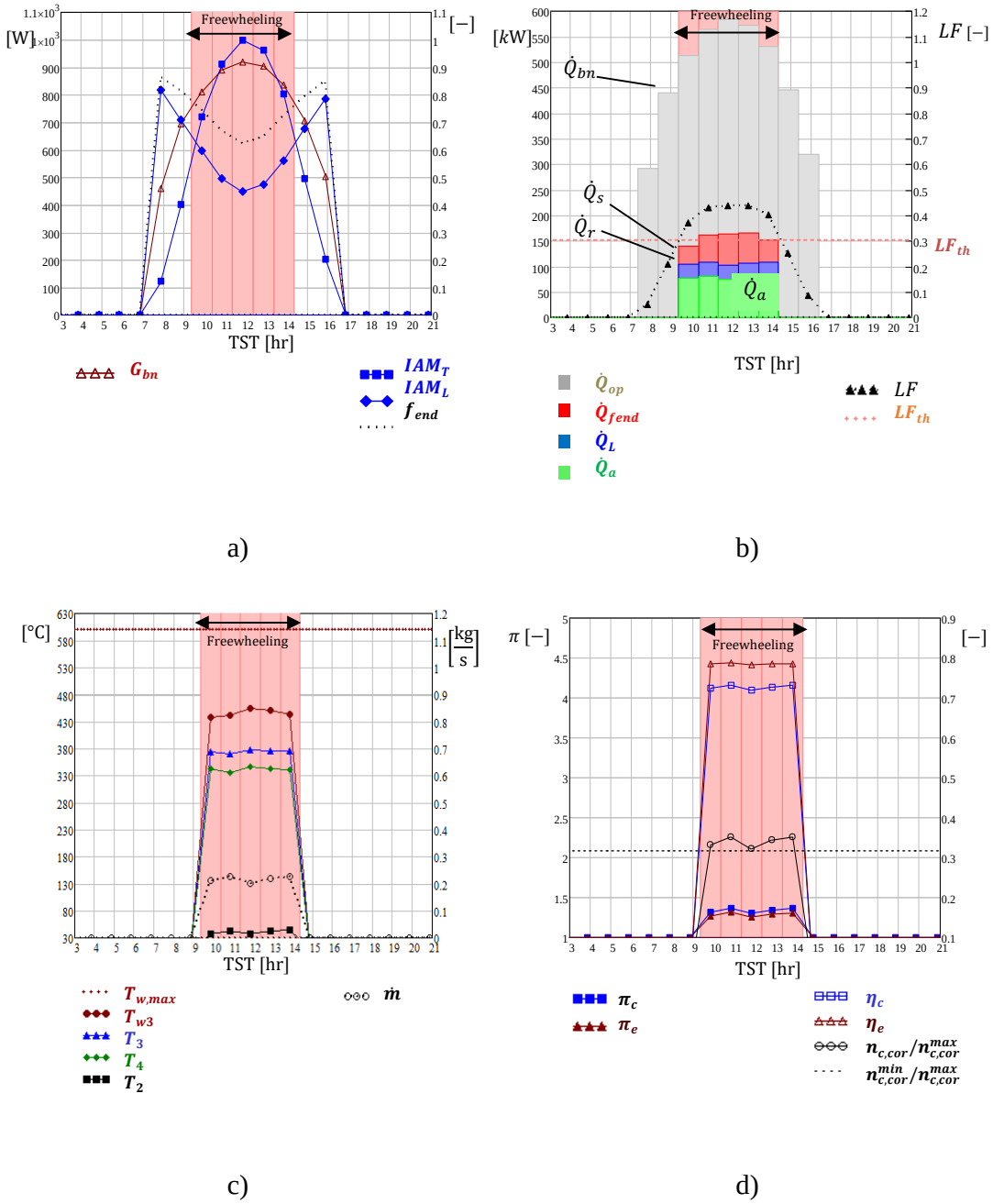

Fig. 4 Performances during a typical winter clear day.

The cases above analyzed show that the T-SAH, without any backup or boost power, can operate during the whole year. However, a drop both in the delivered power and in daily operating hours occur from summer to winter season. During cloudy days the system would have a discontinued operation. The reason is that under low irradiance conditions, the turbocharger is not able to work in freewheeling, and the T-SAH must be considered shut off in the present simulation. Improvements are possible for these shut off conditions. One is straightforward; the turbocharger can be bypassed from the circuit. Then the air is pumped using the auxiliary compressor (Fig.1). This allows producing solar hot air, although consuming auxiliary energy for pumping, which is expected to be low due to the low solar power and low mass flow rate involved. In addition, the integration with external renewable energy sources can be considered, as well as a thermal storage unit.

5. Conclusions

An innovative solar air heater using concentrating Linear Fresnel collectors for industrial application has been presented and analysed in this study. The turbo-assisted solar air heater has been numerically simulated through a steady-state model. This allows to investigate the behaviour of a medium scale facility under a variety of conditions and to identify the relevant design and optimization parameters. The model obtained computes the operational state of the system and hot air production at any hour of the typical meteorological year from a given location.

The results confirm the technical feasibility and interest of the concept. The simulation run for representative clear days shows the main features of the system, indicating that the use of a turbocharger allows obtaining a remarkable steady temperature profile for the delivered airflow during the sunny hours of the day, without consuming external energy for pumping.

The T-SAH facilities so configured can provide hot air between 300 °C and 400 °C during summer, winter and intermediate season of the year for the selected location of Madrid (Spain) with a continental Mediterranean climate. The study offers a platform for demonstration plants design paving the way to more low carbon industries.

6. Numenclature

Latin

A	Aperture surface area [m^2]
ac	Auxiliary compressor
c_p	Air specific heat capacity [J kg^{-1} ℃$^{-1}$]
D	Inner diameter of the receiver tube [m]
F'	Collector efficiency factor [-]
F_R	Collector heat removal factor [-]
f	Darcy friction coefficient [-]. f Function
f_{end}	Optical end losses factor [-]
G_{bn}	Normal beam irradiance [W m^{-2}]
h_a	Air heat transfer coefficient [W m^{-2} ℃$^{-1}$]
IAM	Incidence angle modifier [-]
k	Thermal conductivity [W m^{-1} ℃$^{-1}$]
L	Length [m]
LF	Load factor $\dot{q}_s/\dot{q}_{s,peak}$
$\dot{m}$	Air mass flow rate [kg s^{-1}]
n	Rotating speed [rpm]
n_p	Number parallel U-loops
n_s	Number of modules in series in a U-loop
P	Receiver tube cross-section perimeter [m]
Pr	Prandtl number [-]
p	Pressure [Pa]
$\dot{Q}$	Thermal power [W]
Q	Thermal energy [J]
$\dot{q}_s$	Concentrated solar irradiance [W m^{-2}]
$\dot{q}_u$	Thermal power flux to air [W m^{-2}]
Re	Reynolds number [-]
T	Temperature [K, °C]
TST	True solar time [hr]
U_L	Thermal losses coefficient receiver [Wm^{-2} K^{-1}]
$\dot{W}$	Power [W]
W_a	Rectangular aperture total width [m]

Greek

γ	Isentropic exponent [-]
ρ	Density [kg m^{-3}]
η_{op0}	Maximum optical efficiency [-]
η_m	Mechanical efficiency of turbocharger [-]
η	Total to total isentropic efficiency [-]
π	Pressure ratio [-]

Subscripts

a	Air
amb	Ambient
atm	Atmospheric
bn	Normal beams
c	Compression. Compressor
e	Expansion. Turbine
ex	Receiver tube external surface
$fend$	End optical losses factor
in	Inlet
ou	Outlet
t	Stagnation variable
th	Threshold
tot	Total
T	Turbocharger
w	Wall
0	Inlet from atmosphere
1	Compressor inlet
2	Compressor outlet
3	Turbine inlet
4	Turbine outlet

Superscripts

min	Minimum
max	Maximum

Acronyms

ETC	Evacuated Tube Collector
CSH	Concentrating Solar Heat
HTF	Heat Transfer Fluid
IAM	Incident Angle Modifier
LFC	Linear Fresnel collector
PTC	Parabolic Trough Collector
SAH	Solar Air Heater
SHC	Solar Heating Collectors
SHIP	Solar Heat for Industrial Processes

Others

⟨ ⟩	Functional dependence

θ_L Longitudinal angle [rad]
θ_T Transversal angle [rad]

7. References

Burkholder, F, and C Kutscher. 2008. “Heat-Loss Testing of Solel’s UVAC3 Parabolic Trough Receiver.” *NREL Technical Report* TP-550-423 (January): 19.

Duffie, John A., William A. Beckman, and Jon McGowan. 1985. *Solar Engineering of Thermal Processes*. *American Journal of Physics*. Vol. 53. https://doi.org/10.1119/1.14178.

Famiglietti, A., A. Lecuona-Neumann, J. Nogueira, and M. Rahjoo. 2020. “Direct Solar Production of Medium Temperature Hot Air for Industrial Applications in Linear Concentrating Solar Collectors Using an Open Brayton Cycle. Viability Analysis.” *Applied Thermal Engineering* 169. https://doi.org/10.1016/j.applthermaleng.2020.114914.

Guzzella, Lino, and Christopher H. Onder. 2010. *Introduction to Modeling and Control of Internal Combustion Engine Systems*. https://doi.org/10.1007/978-3-642-10775-7.

Habte, Aron, Thomas Stoffel, Richard Perez, Daryl Myers, Christian Gueymard, Philippe Blanc, and Stefan Wilbert. 2017. “*Best Practices Handbook for the Collection and Use of Solar Resource Data for Solar Energy Applications: Second Edition.*” NREL, no. December 2017: 2.1-2.22. www.nrel.gov/publications.

Heimsath, A., G. Bern, D. Van Rooyen, and P. Nitz. 2014. “Quantifying Optical Loss Factors of Small Linear Concentrating Collectors for Process Heat Application.” *Energy Procedia* 48 (March 2016): 77–86. https://doi.org/10.1016/j.egypro.2014.02.010.

International Energy Agency. 2018. “KEY WORLD ENERGY STATISTICS 2019.”

Karathanasis, Stavros. 2019. *Linear Fresnel Reflector Systems for Solar Radiation Concentration*. *Linear Fresnel Reflector Systems for Solar Radiation Concentration*. https://doi.org/10.1007/978-3-030-05279-9.

Lecuona-Neumann, A. 2016. *Secadero solar*. Patented in Spain P201630068, issued in 2016.

Mekhilef, S., R. Saidur, and A. Safari. 2011. “A Review on Solar Energy Use in Industries.” *Renewable and Sustainable Energy Reviews* 15 (4): 1777–90. https://doi.org/10.1016/j.rser.2010.12.018.

Sharma, Ashish K., Chandan Sharma, Subhash C. Mullick, and Tara C. Kandpal. 2017. “Solar Industrial Process Heating: A Review.” *Renewable and Sustainable Energy Reviews* 78 (December 2016): 124–37. https://doi.org/10.1016/j.rser.2017.04.079.

“SHIP Database.” n.d. http://ship-plants.info/.

Solatom. n.d. “SOLAR STEAM FOR INDUSTRIAL PROCESSES.” http://www.solatom.com/.